14. T. Nishino, M. Miyake, Y. Harada, U. Kawabe, *IEEE Electron Device Lett.* **EDL-6**, 297 (1985).
15. H. Takayanagi, T. Kawakami, *Phys. Rev. Lett.* **54**, 2449 (1985).
16. A. W. Kleinsasser *et al.*, *Appl. Phys. Lett.* **55**, 1909 (1989).
17. C. Nguyen, J. Werking, H. Kroemer, E. L. Hu, *Appl. Phys. Lett.* **57**, 87 (1990).
18. B. D. Josephson, *Phys. Lett.* **1**, 251 (1962).
19. A. F. Andreev, *Zh. Eksp. Theor. Fiz.* **46**, 1823 (1964) [*Sov. Phys. JETP* **19**, 1228 (1964)].
20. B. Pannetier, H. Courtois, *J. Low Temp. Phys.* **118**, 599 (2000).
21. K. Flensberg, J. B. Hansen, M. Octavio, *Phys. Rev. B* **38**, 8707 (1988).
22. A. Chrestin, U. Merkt, *Appl. Phys. Lett.* **70**, 3149 (1997).
23. M. Octavio, M. Tinkham, G. E. Blonder, T. M. Klapwijk, *Phys. Rev. B* **27**, 6739 (1983).
24. E. Scheer *et al.*, *Phys. Rev. Lett.* **86**, 284 (2001).
25. M. R. Buitelaar *et al.*, *Phys. Rev. Lett.* **91**, 057005 (2003).
26. P. A. Lee, A. D. Stone, *Phys. Rev. Lett.* **55**, 1622 (1985).
27. C. W. J. Beenakker, *Phys. Rev. Lett.* **67**, 3836 (1991).
28. B. L. Al'tshuler, B. Z. Spivak, *Zh. Eksp. Theor. Fiz.* **92**, 609 (1987) [*Sov. Phys. JETP* **65**, 343 (1987)].
29. Y. Makhlin, G. Schön, A. Shnirman, *Rev. Mod. Phys.* **73**, 357 (2001).
30. M. J. Storcz, F. K. Wilhelm, *Appl. Phys. Lett.* **83**, 2387 (2003).
31. We thank J. Eroms, R. Schouten, C. Harmans, P. Hadley, Yu. Nazarov, C. Beenakker, T. Klapwijk, B. van Wees, and F. Giazotto. Financial support was obtained from the Dutch Fundamenteel Onderzoek der Materie, the Japanese Solution Oriented Research for Science and Technology program, and the Korean Science and Engineering Foundation.

Supporting Online Material
www.sciencemag.org/cgi/content/full/309/5732/272/DC1
Materials and Methods
Figs. S1 to S4
References

13 April 2005; accepted 25 May 2005
10.1126/science.1113523

Skeleton of *Euplectella* sp.: Structural Hierarchy from the Nanoscale to the Macroscale

Joanna Aizenberg,[1]* James C. Weaver,[2] Monica S. Thanawala,[1] Vikram C. Sundar,[1] Daniel E. Morse,[2] Peter Fratzl[3]

Structural materials in nature exhibit remarkable designs with building blocks, often hierarchically arranged from the nanometer to the macroscopic length scales. We report on the structural properties of biosilica observed in the hexactinellid sponge *Euplectella* sp. Consolidated, nanometer-scaled silica spheres are arranged in well-defined microscopic concentric rings glued together by organic matrix to form laminated spicules. The assembly of these spicules into bundles, effected by the laminated silica-based cement, results in the formation of a macroscopic cylindrical square-lattice cagelike structure reinforced by diagonal ridges. The ensuing design overcomes the brittleness of its constituent material, glass, and shows outstanding mechanical rigidity and stability. The mechanical benefits of each of seven identified hierarchical levels and their comparison with common mechanical engineering strategies are discussed.

Nature fascinates scientists and engineers with numerous examples of exceptionally strong building materials. These materials often show complex hierarchical organization from the nanometer to the macroscopic scale (*1*–*7*). Every structural level contributes to the mechanical stability and toughness of the resulting design. For instance, the subtle interplay between the lattice structure, fibril structure, and cellulose is responsible for the remarkable properties of wood. In particular, it consists of parallel hollow tubes, the wood cells, which are reinforced by nanometer-thick cellulose fibrils wound helically around the cell to adjust the material as needed (*8*). Deformation occurs by shearing of a matrix rich in hemicelluloses and lignin, "gluing" neighboring fibrils, and allowing a stick-slip movement of the fibrils (*9*). Wood is an example that shows the wide range of mechanical performance achievable by constructing with fibers. Bone is another example of a hierarchically assembled fibrous material. Its strength critically depends on the interplay between different structural levels—from the molecular/nanoscale interaction between crystallites of calcium phosphate and an organic framework, through the micrometer-scale assembly of collagen fibrils, to the millimeter-level organization of lamellar bone (*4*, *10*–*12*). Whereas wood is fully organic material, bone is a composite, with about half organic and half mineral components tightly interconnected at the nanoscale. However, nature has also evolved almost pure mineral structures, which—despite the inherent brittleness of most minerals—are tough enough to serve as protection for the organism. In mollusk nacre, for example, the toughening effect is due to well-defined nanolayers of organics at the interfaces between microtablets of calcium carbonate (*5*, *6*). In such structures, the stiff components (usually mineral) absorb the bulk of the externally applied loads. The organic layers, in turn, provide toughness, prevent the spread of the cracks into the interior of the structure, and even confer a remarkable capacity for recovery after deformation (*13*).

Glass is widely used as a building material in the biological world, despite its fragility (*14*–*20*). Organisms have evolved means to effectively reinforce this inherently brittle material. It has been shown that spicules in siliceous sponges exhibit exceptional flexibility and toughness compared with brittle synthetic glass rods of similar length scales (*15*, *20*). The mechanical protection of diatom cells was suggested to arise from the increased strength of their silica frustules (*16*). We have recently described the structural and optical properties of individual spicules of the glass sponge *Euplectella* sp., a deep-sea, sediment-dwelling sponge from the Western Pacific (*21*, *22*). Not only do these spicules have optical properties similar to manufactured optical fibers, but they are also structurally resistant. The individual spicules are, however, just one structural level in a highly sophisticated, nearly purely mineral skeleton of this siliceous sponge (*23*). Here, we discuss the structural hierarchy of the entire skeleton of *Euplectella* sp. from the nanoscale to the macroscale. We show that the assembly of a macroscopic, mechanically resistant cylindrical glass cage is possible in a modular, bottom-up fashion comprising at least seven hierarchical levels, all contributing to mechanical performance. These include silica nanospheres that are arranged into concentric layers separated from one another by alternating organic layers to yield lamellar fibers. The fibers are in turn bundled and organized within a silica matrix to produce flexurally rigid composite beams at the micron scale. The macroscopic arrangement of these beams in a rectangular lattice with ancillary crossbeams is ideal for resisting tensile and shearing stresses. Finally, we identify various structural motifs that provide additional structural benefits to this unique glass skeletal system.

Figure 1A is a photograph of the entire skeleton of *Euplectella* sp., showing the intricate, cylindrical cagelike structure (20 to 25 cm long, 2 to 4 cm in diameter) with lateral ("oscular") openings (1 to 3 mm in diameter). The diameter of the cylinder and the size of the oscular openings gradually increase from the bottom to the top of the structure. The basal segment of *Euplectella* sp. is anchored into the soft sediments of the sea floor and is loosely connected to the rigid cage structure, which is

[1]Bell Laboratories/Lucent Technologies, Murray Hill, NJ 07974, USA. [2]Institute for Collaborative Biotechnologies and Materials Research Laboratory, University of California, Santa Barbara, CA 93106, USA. [3]Max Planck Institute of Colloids and Interfaces, D-14424 Potsdam, Germany.

*To whom correspondence should be addressed. E-mail: jaizenberg@lucent.com

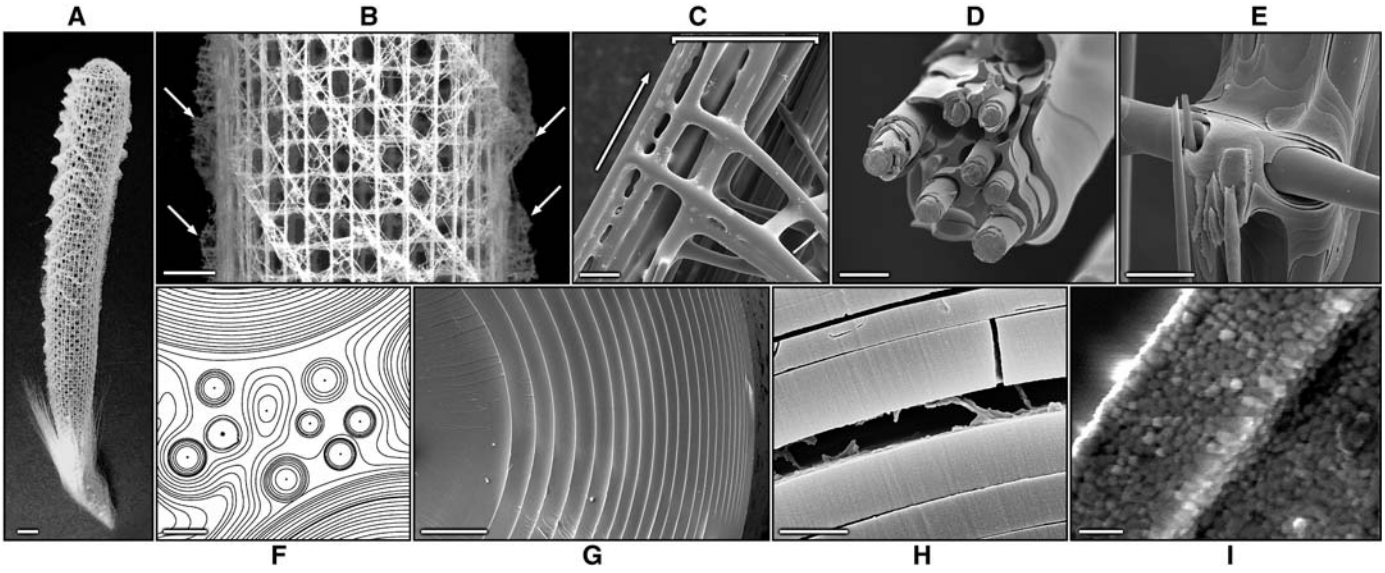

Fig. 1. Structural analysis of the mineralized skeletal system of *Euplectella* sp. (**A**) Photograph of the entire skeleton, showing cylindrical glass cage. Scale bar, 1 cm. (**B**) Fragment of the cage structure showing the square-grid lattice of vertical and horizontal struts with diagonal elements arranged in a chessboard manner. Orthogonal ridges on the cylinder surface are indicated by arrows. Scale bar, 5 mm. (**C**) Scanning electron micrograph (SEM) showing that each strut (enclosed by a bracket) is composed of bundled multiple spicules (the arrow indicates the long axis of the skeletal lattice). Scale bar, 100 μm. (**D**) SEM of a fractured and partially HF-etched (*25*) single beam revealing its ceramic fiber-composite structure. Scale bar, 20 μm. (**E**) SEM of the HF-etched (*25*) junction area showing that the lattice is cemented with laminated silica layers. Scale bar, 25 μm. (**F**) Contrast-enhanced SEM image of a cross section through one of the spicular struts, revealing that they are composed of a wide range of different-sized spicules surrounded by a laminated silica matrix. Scale bar, 10 μm. (**G**) SEM of a cross section through a typical spicule in a strut, showing its characteristic laminated architecture. Scale bar, 5 μm. (**H**) SEM of a fractured spicule, revealing an organic interlayer. Scale bar, 1 μm. (**I**) Bleaching of biosilica surface revealing its consolidated nanoparticulate nature (*25*). Scale bar, 500 nm.

exposed to ocean currents and supports the living portion of the sponge responsible for filtering and metabolite trapping (*23*, *24*). The characteristic sizes and construction mechanisms of the *Euplectella* sp. skeletal system are expected to be fine-tuned for these functions.

At the macroscale, the cylindrical structure is reinforced by external ridges that extend perpendicular to the surface of the cylinder and spiral the cage at an angle of 45° (shown by arrows in Fig. 1B). The pitch of the external ridges decreases from the basal to the top portion of the cage. The surface of the cylinder consists of a regular square lattice composed of a series of cemented vertical and horizontal struts (Fig. 1B), each consisting of bundled spicules aligned parallel to one another (Fig. 1C), with diagonal elements positioned in every second square cell (Fig. 1B). Cross-sectional analyses of these beams at the micron scale reveal that they are composed of collections of silica spicules (5 to 50 μm in diameter) embedded in a layered silica matrix (Fig. 1, D to F). The higher solubility of the cement when treated with hydrofluoric acid (HF) (*25*), compared with the underlying spicules, suggests that the cement is composed of more hydrated silica (Fig. 1, D and E). The constituent spicules have a concentric lamellar structure, with the layer thickness decreasing from ~1.5 μm at the center of the spicule to ~0.2 μm at the spicule periphery (Fig. 1G). These layers are arranged in a cylindrical fashion around a central proteinaceous filament and are separated from one another by organic interlayers (Fig. 1H). Etching of spicule layers and the surrounding cement showed that at the nanoscale the fundamental construction unit consists of consolidated hydrated silica nanoparticles (50 to 200 nm in diameter) (Fig. 1I) (*17*–*19*, *22*). The different levels of structural complexity are schematically shown in Fig. 2. In the following discussion, each hierarchical level is examined from the mechanical perspective.

The first level is biologically produced glass composed of consolidated silica nanospheres formed around a protein filament (Fig. 2A). Glass as a building material suffers primarily from its brittleness. This means that its strength is limited mostly by surface defects where the applied stresses concentrate. A scratch in the surface of glass readily induces fracture. If we consider that surface defects in the biosilica may be induced by external point loads, either biologically or otherwise applied, a scratched plain glass spicule would lose most of its strength and would fracture when subsequently loaded in tension or bending. This can be expressed quantitatively by the well-known Griffith law, which relates the strength σ_f to the size of the largest defect, h, for $h \geq h^*$, as

$$\sigma_f = \frac{K_{1C}}{\sqrt{\pi h}} \approx \sigma_f^{th}\sqrt{\frac{h^*}{h}} \qquad \text{(Eq. 1)}$$

where K_{1C} is the fracture toughness of the glass, σ_f^{th} is the theoretical strength of the defect-free material, and h^* is a characteristic length (for typical ceramic materials, this length is on the order of 10 to 30 nm) (*26*). For defects smaller than h^*, there is no stress concentration at the defect, and the strength of the material is equal to its defect-free value (*26*). Because the mineral particles in bone, for example, are thinner than this value, these particles should be insensitive to defects and therefore flaw tolerant. This argument does not apply, however, to biologically produced glass, because individual silica nanospheres range from 50 nm to 200 nm in diameter and thus are larger than h^*.

The intrinsically low strength of the glass is balanced at the next structural level. The spicule as a whole can be regarded as a laminated composite (*27*) in which the organic interlayers act as crack stoppers (Fig. 2B). If a point load is applied to the surface, one may expect that the damage will be restricted to the outermost layers (*28*). A larger number of individual glass layers should protect the spicule more effectively from this type of damage. Thin organic interlayers seem also to be important to prevent cracks from propagating to inner layers under the influence of indentation (*28*). The observed decrease of the silica layer thickness from the spicule core to the periphery is likely to provide an additional reinforcement to the spicules. Thicker inner layers help enhance mechanical rigidity of the

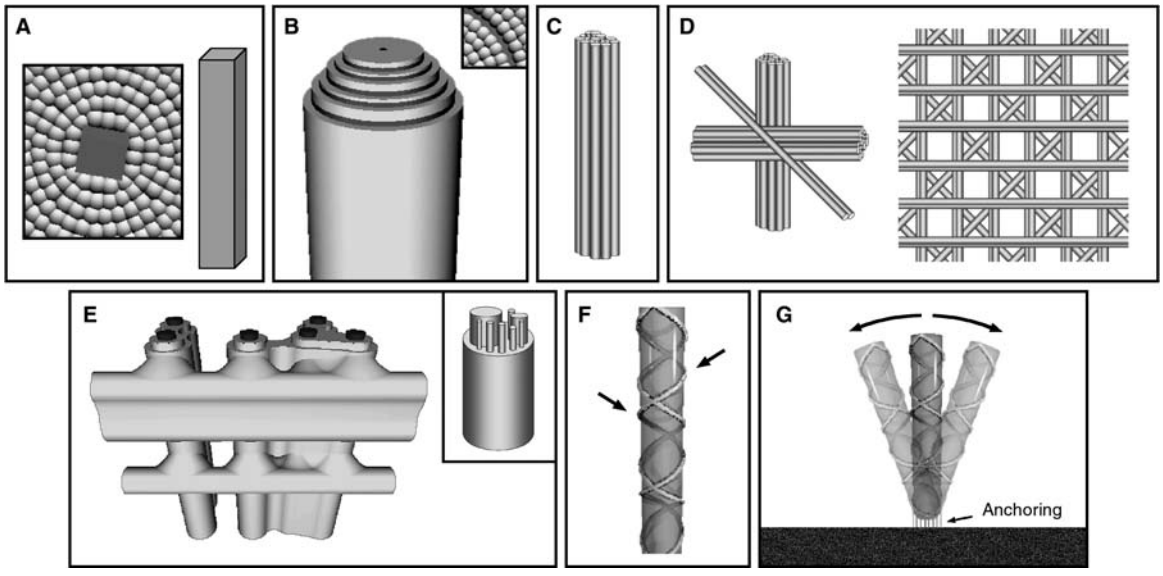

Fig. 2. Proposed scheme summarizing the seven levels of structural hierarchy in the skeletal system of *Euplectella* sp. (**A**) Consolidated silica nanoparticles deposited around a preformed organic axial filament (shown on the right). (**B**) Lamellar structure of spicule made of alternating organic and silica layers. Inset depicts the organically glued interlayer region. (**C**) Bundling of spicules. (**D**) (Right) Vertical and horizontal ordering of bundled spicules forming a square-lattice cylindrical cage with every second cell reinforced by diagonal elements (see Eq. 2). (Left) The node structure. (**E**) Cementation of nodes and spicules in the skeletal lattice with layered silica matrix. (Inset) Fiber-reinforced composite of an individual beam in the strut. (**F**) Surface ridges protect against ovalization of the skeleton tube. (**G**) Flexural anchoring of the rigid cage into the soft sediments of the sea floor.

spicule, whereas the thinner outer layers effectively limit the depth of crack penetration. The crack deviation by organic interlayers in laminated spicules can be clearly seen in Fig. 3.

In a further level of hierarchy, spicules are joined into parallel bundles (Fig. 2C), a well-known construction principle in ceramic materials (*29*). Generally, a bundle of fibers with slightly different strength will have a much larger defect tolerance (and, therefore, strength) than each of the individual fibers. Indeed, if one fiber fails (e.g., under tension), neighboring ones still hold, and the crack in the first fiber will be deflected at the interface to its neighbors (or at the interface between the fiber and cement). A weak lateral bonding between fibers (or between fiber and matrix) is essential for this toughening mechanism to work (*30*).

The bundled spicules are arranged horizontally and vertically into a square-grid cylindrical cage reinforced by ancillary diagonal fibers running in both directions (Fig. 2D). Theoretical analyses of strut structures have shown that when the number of struts per node, Z, exceeds a certain value, the structure is stable even if the nodes can rotate freely. Deshpande *et al*. (*31*) have given the stability limit as

$$Z \geq 6\,(D - 1) \qquad \text{(Eq. 2)}$$

for grids in $D = 2$ or in $D = 3$ dimensions. A simple square grid made of fibers (with $D = 2$ and $Z = 4$) is clearly unstable with respect to shear when the nodes can rotate freely. In cases where a free rotation of the nodes is not possible, the shear stability of the simple square grid is limited by the bending moments, which the nodes and struts can withstand. However, cellular structures are usually much stronger when the struts are loaded in tension rather than in bending (*32*). Hence, structures fulfilling inequality (Eq. 2), where any type of loading will result in tension and compression of the fibers only, are likely to be stronger. In the *Euplectella* skeletal system, three main spicular struts (horizontal, vertical, and one of the two possible diagonals) are joined in every node of the square grid, which means that $Z = 6$. This is just sufficient to fulfill Eq. 2 for a two-dimensional grid. Most remarkably, every second square in the skeletal lattice is left without a diagonal fiber. By adding the crossbeams in these empty squares, the number Z would jump to 8, which would be an overdesign in terms of Eq. 2, with no apparent structural advantages for the prevention of shear stresses.

Hierarchical levels shown in Fig. 2, A to D, describe the structure of the *Euplectella* skeletal system at its early stages of development [the "flexible phase" (*24*)]. During maturation, the flexible cage is rigidified into a "stiff sponge" (*24*) as a result of the use of two additional levels of structural hierarchy. All the fibers become joined at the nodes of the square grid with silica cement that effectively coats the entire skeletal lattice (Fig. 2E) and thus forms the matrix of a ceramic fiber composite. The only exception is the region where basalia (anchor spicules) emerge from the base of the composite structure. It is also noteworthy that the cement itself exhibits a laminated architecture (Fig. 1, D to F) that hinders crack propagation through this silica matrix.

The resultant rigid structure ensures that the sheet forming the cylinder is very stable in two dimensions with a number of measures to reduce the intrinsic brittleness of glass. Finally, the cylindrical cage must also be stable in three dimensions, and the main limitation is the ovalization of the cylinder, which reduces the bending stability of the tubelike cage. In this sense, it is very likely that the helical ridges around the skeleton of *Euplectella* sp. (Fig. 2F), in conjunction with the consolidating silica matrix discussed above, serve primarily a mechanical function in preventing ovalization of the sponge skeleton. This argument is further supported by the fact that the ridges are absent in the narrow bottom portion of the tube and ap-

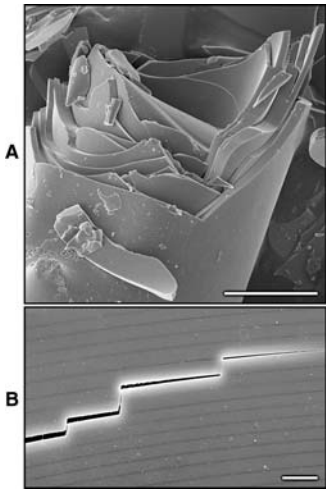

Fig. 3. Fracture surfaces in the spicules from *Euplectella* sp. (**A**) SEM of a fractured laminated spicule. (**B**) Examination of a polished cross section of the spicule from a related species clearly reveals crack deviation by the organic layers. Scale bars for both micrographs, 10 μm.

pear in the middle region where the sponge diameter increases beyond a specific point. To ensure the stability of the tube with the vertically growing diameter, there is a distinct increase of the surface density and thickness of the external ridges in the upper regions of the skeletal system (Fig. 1A) (*23*, *24*).

Exposed to currents, the elevated rigid sponge cage attached to the ocean floor will experience bending stresses that are concentrated at the anchor point. Two mechanical strategies may counteract the stress concentration: to stiffen the anchor point, which will withstand bending forces up to a certain limit and then break, or to make the anchor very flexible. The sponge uses the latter strategy by loosely incorporating the basalia (anchor) spicules into the vertical struts of the rigid cage (Fig. 2G). The advantage of this strategy is that there is no limiting stress from currents, and the cage swings freely in the ocean because of the inherent flexibility of the individual spicules that form the connection.

The structural complexity of the glass skeleton in the sponge *Euplectella* sp. is an example of nature's ability to improve inherently poor building materials. The exceptional mechanical stability of the skeleton arises from the successive hierarchical assembly of the constituent glass from the nanometer to the macroscopic scale. The resultant structure might be regarded as a textbook example in mechanical engineering, because the seven hierarchical levels in the sponge skeleton represent major fundamental construction strategies such as laminated structures, fiber-reinforced composites, bundled beams, and diagonally reinforced square-grid cells, to name a few (*33*). We conclude that the *Euplectella* sp. skeletal system is designed to provide structural stability at minimum cost, a common theme in biological systems where critical resources are often limited. We believe that the study of the structural complexity of unique biological materials and the underlying mechanisms of their synthesis will help us understand how organisms evolved their sophisticated structures for survival and adaptation and ultimately will offer new materials concepts and design solutions.

References and Notes

1. S. A. Wainwright, W. D. Biggs, J. D. Currey, J. M. Gosline, *Mechanical Design in Organisms* (Wiley, New York, 1976).
2. J. D. Currey, *J. Exp. Biol.* **202**, 3285 (1999).
3. H. A. Lowenstam, S. Weiner, *On Biomineralization* (Oxford Univ. Press, Oxford, 1989).
4. S. Weiner, H. D. Wagner, *Annu. Rev. Mater. Sci.* **28**, 271 (1998).
5. S. Kamat, X. Su, R. Ballarini, A. H. Heuer, *Nature* **405**, 1036 (2000).
6. A. G. Evans *et al.*, *J. Mater. Res.* **16**, 2475 (2001).
7. G. Mayer, M. Sarikaya, *Exp. Mech.* **42**, 395 (2002).
8. H. Lichtenegger, A. Reiterer, S. E. Stanzl-Tschegg, P. Fratzl, *J. Struct. Biol.* **128**, 257 (1999).
9. J. Keckes *et al.*, *Nat. Mater.* **2**, 810 (2003).
10. P. Fratzl, H. S. Gupta, E. P. Paschalis, P. Roschger, *J. Mater. Chem.* **14**, 2115 (2004).
11. A. E. Porter, L. W. Hobbs, V. B. Rosen, M. Spector, *Biomaterials* **23**, 725 (2002).
12. T. Hassenkam *et al.*, *Bone* **35**, 4 (2004).
13. B. L. Smith *et al.*, *Nature* **399**, 761 (1999).
14. C. C. Perry, T. Keeling-Tucker, *J. Biol. Inorg. Chem.* **5**, 537 (2000).
15. C. Levi, J. L. Barton, C. Guillemet, E. Le Bras, P. Lehuede, *J. Mater. Sci. Lett.* **8**, 337 (1989).
16. C. E. Hamm *et al.*, *Nature* **421**, 841 (2003).
17. J. N. Cha *et al.*, *Proc. Natl. Acad. Sci. U.S.A.* **96**, 361 (1999).
18. N. Kroger, S. Lorenz, E. Brunner, M. Sumper, *Science* **298**, 584 (2002).
19. J. C. Weaver *et al.*, *J. Struct. Biol.* **144**, 271 (2003).
20. M. Sarikaya *et al.*, *J. Mater. Res.* **16**, 1420 (2001).
21. V. C. Sundar, A. D. Yablon, J. L. Grazul, M. Ilan, J. Aizenberg, *Nature* **424**, 899 (2003).
22. J. Aizenberg, V. C. Sundar, A. D. Yablon, J. C. Weaver, G. Chen, *Proc. Natl. Acad. Sci. U.S.A.* **101**, 3358 (2004).
23. F. E. Schulze, *Report on the Hexactinellida Collected by H. M. S. Challenger During the Years 1873-1876*, vol. XXI (Berlin, 1887).
24. T. Saito, I. Uchida, M. Takeda, *J. Zool.* **258**, 521 (2002).
25. HF treatment and bleaching experiments: Small sections (2 cm by 2 cm) of the *Euplectella* sp. skeletal lattice were soaked for 10 min in 5 M NH_4F:2.5 M HF or 2.5% NaOCl solution, respectively. The remaining skeletal material was removed, rinsed with water and 95% ethanol, dried, and prepared for examination by scanning electron microscope.
26. H. J. Gao, B. H. Ji, I. L. Jager, E. Arzt, P. Fratzl, *Proc. Natl. Acad. Sci. U.S.A.* **100**, 5597 (2003).
27. M. Seshadri, S. J. Bennison, A. Jagota, S. Saigal, *Acta Mater.* **50**, 4477 (2002).
28. H. Chai, B. R. Lawn, *Acta Materialia* **50**, 2613 (2002).
29. W. J. Clegg, K. Kendall, N. M. Alford, T. W. Button, J. D. Birchall, *Nature* **347**, 455 (1990).
30. K. T. Faber, *Annu. Rev. Mater. Sci.* **27**, 499 (1997).
31. V. S. Deshpande, M. F. Ashby, N. A. Fleck, *Acta Materialia* **49**, 1035 (2001).
32. L. J. Gibson, M. F. Ashby, *Cellular Solids: Structure and Properties* (Cambridge University Press, ed. 2, 1999).
33. G. Mayer, *Ceram. Bull.* **83**, 9305 (2004).

34. We thank M. Ilan, G. E. Fantner, D. Kisailus, and M. J. Porter for their help. J.C.W. and D.E.M. were supported by grants from NASA (NAG1-01-003 and NCC-1-02037), the Institute for Collaborative Biotechnologies through grant DAAD19-03D-0004 from the Army Research Office, and the NOAA National Sea Grant College Program, U.S. Department of Commerce (NA36RG0537, Project R/MP-92) through the California Sea Grant College System.

14 March 2005; accepted 4 May 2005
10.1126/science.1112255

Isolation of Two Seven-Membered Ring C_{58} Fullerene Derivatives: $C_{58}F_{17}CF_3$ and $C_{58}F_{18}$

Pavel A. Troshin,[1] Anthony G. Avent,[2] Adam D. Darwish,[2] Natalia Martsinovich,[2] Ala'a K. Abdul-Sada,[2] Joan M. Street,[3] Roger Taylor[2]*

Fluorination of C_{60} at 550°C leads to milligram quantities of two stable fullerene derivatives with 58-carbon cage structures: $C_{58}F_{18}$ and $C_{58}F_{17}CF_3$. The compounds were characterized by mass spectrometry and fluorine nuclear magnetic resonance spectroscopy, and the data support a heptagonal ring in the framework. The resulting strain, which has hindered past attempts to prepare these smaller quasi-fullerenes, is mitigated here by hybridization change of some of the carbons in the pentagons from sp^2 to sp^3 because of fluorine addition. The loss of carbon from C_{60} is believed to occur via sequential fluorine addition to a C–C single bond and an adjacent C=C bond, followed by loss of a $:CF_2$ carbene.

Numerous papers describe the structure and properties of fullerenes larger than C_{60} and C_{70} and their derivatives (*1*). The stability of these compounds has been explained by the low strain inherent in a framework of pentagonal carbon rings surrounded by hexagons. By contrast, smaller fullerenes violate this nonadjacent pentagon rule and accordingly have been hard to prepare. Examples comprise the recent isolation of $C_{50}Cl_{10}$ (*2*) and a controversial report of C_{36} (*3*, *4*).

The possibility of fullerenes having seven- as well as five- and six-membered rings (quasi-fullerenes) was first proposed in 1992 (*5*). The structure of C_{58} requires a seven-membered ring produced by removal from C_{60} of a 6:5 bond, that is, one shared by a pentagon and a hexagon (*6*, *7*). The resultant C_{58} structure violates the strain-based nonadjacent pentagon rule (*8*), but a C_{58} derivative will be less strained because of the presence of sp^3 carbons and isolation ought to be feasible (*6*). Both phenylated and methylated C_{58} fragment ions have been observed in electron impact (EI) mass spectrometry of corresponding C_{60} precursors, together with C_{58}/C_{60} ion intensity ratios of up to 76% (*9*–*13*). A C_{58}

[1]Institute of Problems of Chemical Physics of Russian Academy of Sciences, Chernogolovka 142432, Russia. [2]Chemistry Department, Sussex University, Brighton BN1 9QJ, UK. [3]School of Chemistry, University of Southampton, Southampton SO17 1BJ, UK.

*To whom correspondence should be addressed. E-mail: R.Taylor@sussex.ac.uk